ARTICLES

Inclusion of local structure effects in theoretical x-ray resonant scattering amplitudes using *ab initio* x-ray-absorption spectra calculations

J. O. Cross*
Naval Research Laboratory, Washington, D.C. 20375

M. Newville†
Lawrence Livermore National Laboratory, Livermore, California 94550

J. J. Rehr and L. B. Sorensen
University of Washington, Seattle, Washington 98195

C. E. Bouldin
National Institute of Standards and Technology, Gaithersburg, Maryland 20899

G. Watson
University of Maryland Baltimore County, Baltimore, Maryland 21250

T. Gouder and G. H. Lander
European Commission, Joint Research Center, Institute for Transuranium Elements, Postfach 2340, D-76125 Karlsruhe, Germany

M. I. Bell
Naval Research Laboratory, Washington, D.C. 20375
(Received 9 February 1998)

Improved calculations of Bragg peak intensities near atomic resonance are obtained by including the effect of the local environment around the resonant atoms on the resonant scattering amplitudes $\Delta f = f' + if''$. Theoretical absorption cross sections calculated by the *ab initio* x-ray-absorption code FEFF are used to obtain the imaginary part f'' by extension of the optical theorem to nonforward scattering under the dipole approximation. The real part f' is obtained by a limited range Kramers-Kronig transform of the difference between f'' based on FEFF and existing theoretical calculations of f'' based on an isolated-atom model. The atomic part of Δf calculated by FEFF for the resonant atom embedded in the local potential is assumed to have spherical symmetry; however, no restriction is placed on the spectral features due to multiple scattering of the intermediate-state *virtual* photoelectron. Bragg peak intensities calculated in the kinematic approximation using the FEFF-based Δf are compared to intensities calculated using the isolated-atom Δf and to experimental data for Cu metal and $YBa_2Cu_3O_{6.8}$ at the Cu K absorption edge, and for UO_2 at the U M_{IV} absorption edge. [S0163-1829(98)06541-2]

I. INTRODUCTION

Resonant x-ray scattering is a rapidly expanding field encompassing a wide range of research topics.[1] Development in this area has been stimulated by the availability of synchrotron radiation and by the recognition that scattering near atomic resonances provides large, chemically specific contrast in the scattering amplitudes. For example, the ability to differentiate the contribution of a subset of heavy atoms to the diffraction pattern of a macromolecular crystal using multiple-wavelength anomalous dispersion (MAD), in which measurements are made at a few energies carefully chosen with respect to the resonance, has revolutionized the field of protein crystallography.[2,3] Recently, with the development of diffraction anomalous fine structure (DAFS),[4–6] resonant x-ray diffraction as a continuous function of energy has been shown to provide additional information about the local structural, electronic, and magnetic environment of the resonant atoms that complements the information about the long-range structural, electronic, and magnetic order provided by other diffraction techniques.

With the increase in the availability of synchrotron radiation, resonant x-ray-scattering experiments have become more practical and the need for accurate theoretical calculations of the resonant scattering amplitudes $\Delta f = f' + if''$ has become more important. Existing calculations of Δf based on isolated-atom models[7,8] are able to reproduce the gross spectral features, i.e., the cusp in f' and the step in f'', and tables of these calculations are standard tools for the analysis of experimental data; however, the isolated-atom models do

not take into consideration the effects of the local environment around the resonant atom and therefore fail to reproduce many important additional spectral features observed in Δf, such as the *white line* at certain absorption edges,[9] angular variation induced by crystal symmetry,[10] and the extended fine-structure oscillations which persist for several hundred eV above the absorption edge.[5]

It is well known from x-ray-absorption spectroscopy (XAS) that the features observed in the absorption cross section near a core electron resonance reflect the density of final states available to the outgoing photoelectron and depend strongly on the local environment in which the resonant atom is embedded.[11] Extensive work has been done in the last 20 years to develop a real-space photoelectron-scattering path formalism which describes XAS in terms of the local physical, chemical, and electronic environment of the resonant atoms.[12] More recently, improved theoretical understanding has allowed the development of general-purpose *ab initio* calculations, such as those implemented in the computer program FEFF,[13,14] which accurately reproduce nearly all of the features observed in the absorption cross sections. Because of the close mathematical relationship between the matrix elements for absorption and for resonant elastic scattering, the scattering path formalism developed for calculating XAS has immediate application to including the effects local structure in theoretical calculations of Δf for resonant x-ray scattering.

This paper describes application of the x-ray-absorption code FEFF to improving existing calculations of Δf, including the polarization dependence of spectral features induced by the local environment. In addition to providing a first-principles approach to calculating Δf, which is useful for understanding the origin of the spectral features, the output of FEFF is easily separated into contributions from individual scattering paths that are parametrized in terms of structural variables, such as path length, disorder, and amplitude, and can be optimized in a least-squares fit to resonant x-ray-scattering data. Although we have applied this work specifically to modeling DAFS data, the results should be useful for other resonant x-ray-scattering applications as well.

II. THEORY

A. X-ray scattering and x-ray absorption

Some examination of the relationship between absorption and scattering is necessary for extending theoretical calculations of x-ray-absorption cross sections to modeling resonant x-ray-scattering amplitudes. In particular, the extension of the optical theorem to nonforward scattering requires justification, and the interpretation of diffraction fine structure in terms of the x-ray-absorption fine-structure (XAFS) photoelectron-scattering path formalism warrants special attention. This section gives a sketch of the relationship between the XAFS and Δf matrix elements, and between real and virtual photoelectron-scattering fine structure in XAFS and DAFS, respectively. A complete derivation of the formal expressions for photon-atom interactions can be found in most advanced treatments of quantum electrodynamics[15] and detailed descriptions of the model used by FEFF for calculating the absorption cross sections can be found in the literature.[14] For simplicity in this discussion, we will use a nonrelativistic formalism, although the FEFF code itself includes the dominant relativistic corrections, i.e., relativistic matrix elements and semirelativistic scattering phase shifts.

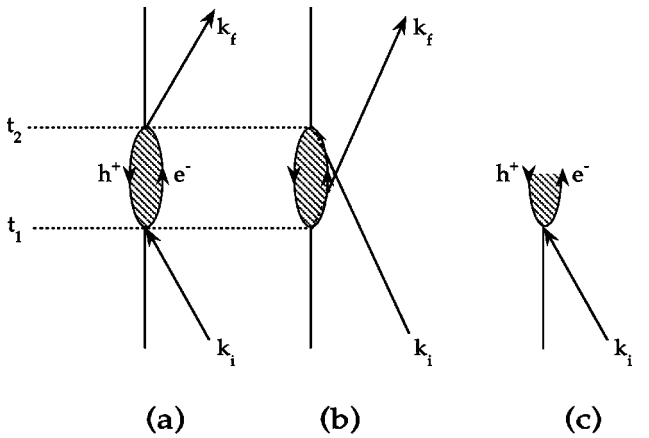

FIG. 1. Feynman diagrams for resonant elastic scattering and absorption. (a) The dominant contribution to resonant scattering can be thought of as the absorption of the incident photon, creating an excited intermediate state, followed by the emission of the outgoing photon. The outgoing photon has the same energy as, and is coherent with, the incident photon. (b) The smaller contribution to resonant scattering, in which the final photon is emitted before the incident photon is absorbed, is negligible near resonance. (c) Absorption is a single-photon process; however, the final states available to the outgoing real photoelectron created by absorption are identical to the states available to the intermediate *virtual* photoelectron in resonant scattering.

From the perturbation expansion of the interaction Hamiltonian, the resonant correction Δf to the Thomson scattering amplitude f_0 is second order in the vector potential and may be written in the dipole approximation as

$$\Delta f(\hbar\omega)=\left(\frac{e}{mc}\right)^2\sum_n \frac{\langle\psi_f|\hat{\mathbf{e}}'^*\cdot\mathbf{r}'|\psi_n\rangle\langle\psi_n|\hat{\mathbf{e}}\cdot\mathbf{r}|\psi_i\rangle}{E_n-\left(E_i+\hbar\omega+\frac{1}{2}i\Gamma_n\right)}+\text{c.c.} \tag{1}$$

where $\hat{\mathbf{e}}$ is the photon polarization vector, $\hat{\mathbf{r}}$ is the dipole operator, e is the electron charge unit, m is the electron mass, c is the speed of light, and c.c. stands for the complex conjugate. In the single-particle approximation, the sum is over all intermediate states ψ_n, with energy E_n, available to a *virtual* photoelectron excited by the incident photon with energy $\hbar\omega$. All of the radiation damping effects are lumped into the intermediate-state lifetime Γ. For elastic scattering, the initial and final states of the bound core electron are equal $\psi_i=\psi_f$. The photon wave vector changes direction, but the photon energy is unchanged, and the scattered photon is coherent with the incident photon.

The dominant contribution to Δf, shown in Fig. 1(a), can be thought of as absorption of the incident photon, creating an intermediate excited state, followed by emission of the outgoing photon. The complex conjugate, shown in Fig. 1(b), can be thought of as emission of the outgoing photon followed by absorption of the incident photon. The complex conjugate is smaller than the dominant term by a factor of the order of $\Gamma/4\hbar\omega$ at resonance, or around 10^{-4} for the Cu

K shell, and can be neglected in the treatment of resonant scattering data. Note that Δf depends on both of the polarization states $\hat{\mathbf{e}}$ and $\hat{\mathbf{e}}'$ for the incident and outgoing photons, even though it has no direct dependence on the incident and outgoing photon wave vectors $\mathbf{k}$ and $\mathbf{k}'$ in the dipole approximation.

In comparison to the resonant scattering described by Eq. (1), the absorption amplitude is first order in the vector potential. In the single-particle approximation, the incident photon is absorbed by a single bound atomic electron. The excited atom in the final state can decay via several channels, but the decay products are incoherent with the initial photon. The total absorption cross section is equal to the squared magnitude of the amplitude summed over all of the final states available to the outgoing photoelectron and may be written, again in the dipole approximation, as

$$\mu(\hbar\omega)=\frac{4\pi^2\hbar\alpha}{\omega m^2}\sum_f \langle\psi_i|\hat{\mathbf{e}}^*\cdot\mathbf{r}'|\psi_f\rangle\langle\psi_f|\hat{\mathbf{e}}\cdot\mathbf{r}|\psi_i\rangle \times\delta(E_f-(E_i+\hbar\omega)). \tag{2}$$

The final states ψ_f available to the photoelectron in Eq. (2) are the same wave functions as the intermediate states ψ_n available to the virtual photoelectron in Eq. (1). Furthermore, because $\psi_i=\psi_f$ in Eq. (1), the theoretical and computational tools used for calculating the matrix elements for the absorption cross section are immediately applicable to calculating the matrix elements for resonant elastic scattering.

Figure 1(c) shows the Feynman diagram representing the absorption amplitude for comparison with the diagrams of Figs. 1(a) and 1(b) for the scattering amplitude. The diagram for the dominant resonant scattering term, Fig. 1(a), can be constructed from the diagram of Fig. 1(c) by *unfolding* it about the midpoint, corresponding to the mathematical operation of multiplying the matrix element represented by Fig. 1(c) by its complex conjugate; however, we emphasize that the polarization state $\hat{\mathbf{e}}$ and its conjugate $\hat{\mathbf{e}}^*$ in Eq. (2) refer to *a single photon*, while the polarization states $\hat{\mathbf{e}}$ and $\hat{\mathbf{e}}'^*$ in Eq. (1) refer to *two different photons*. The DAFS polarization dependence for any particular photoelectron-scattering path will differ from the XAFS polarization dependence for the same path unless the polarization is unchanged by the scattering event. In the absence of dichroism, this condition is met when the wave vector transfer is restricted to lie in the plane normal to $\hat{\mathbf{e}}$, i.e., for σ-σ scattering, and we assume this condition for the experimental examples given below.

Analogous to the standard treatment of XAFS, it is convenient to write Δf as the sum of an atomic contribution Δf_a, due to the resonant atom only, and a photoelectron-scattering contribution χ, which contains all of the fine structure due to photoelectron scattering from the neighbor atoms. The total anomalous scattering amplitude has the form

$$\Delta f=\Delta f_a+f_c''\chi, \tag{3}$$

where Δf_a is the *atomic* part of the resonant scattering amplitude with no photoelectron-scattering terms, f_c'' is the imaginary part of Δf_a due solely to the excited core electron, and all of the photoelectron scattering is relegated to the complex fine-structure function $\chi=\chi'+i\chi''$. Note that we make a distinction between the contribution to Δf_a from the electrons in the excited core electron Δf_c and the contributions to Δf_a from off-resonance electrons in all other shells Δf_{off}:

$$\Delta f_a=\Delta f_{\text{off}}+\Delta f_c. \tag{4}$$

The steplike coefficient $f_c''=\text{Im}[\Delta f_c]$ of χ in Eq. (3) is zero below the absorption edge and sets the scale of the fine-structure amplitude relative to the step height, corresponding to the background function μ_0 in XAFS:

$$\mu=\mu_0(1+\chi_{\text{XAFS}}), \tag{5}$$

where $\chi_{\text{XAFS}}=\text{Im}[\chi(E,\mathbf{Q}=0)]$. The coefficients f_c'' and μ_0 in Eqs. (3) and (5) separate out of the sum over photoelectron-scattering paths in the Green's function formalism used by FEFF to calculate the matrix elements. Since the use of the imaginary part of Δf_c as the coefficient for both the real *and* imaginary parts of χ may not be obvious, a brief derivation is given in the Appendix.

B. Difference Kramers-Kronig transform

While FEFF calculates μ_0 for the core electron, corresponding to f_c'', and both the phase and amplitude of χ, it does not at this time calculate f_a' or μ_{off} from the off-resonance electron shells. We use tabulated atomic calculations[16,44] based on the method of Cromer and Liberman[8] (CL) as background functions; however, because Δf_a and Δf_c in Eq. (3) and Eq. (4) refer to the atom *embedded* in its local environment, it is not sufficient to simply add the FEFF $f_c''\chi$ to the CL Δf_a. For example, compare the CL-based bare atom f_a'' and the FEFF-based embedded atom f_a'' in Fig. 2(a) for fcc Cu at the Cu K absorption edge and in Fig. 2(b) for UO_2 at the U M_{IV} absorption edge. In order to incorporate all of the embedded-atom features in Δf_a, we use a difference form of the Kramers-Krönig (KK) dispersion relations to generate the real part of Δf.

The imaginary part of the resonant elastic scattering amplitude in the forward direction $f''(E=\hbar\omega)=\text{Im}[\Delta f(\hbar\omega;\mathbf{k}=\mathbf{k}')]$ is related to the total absorption cross section $\mu(\hbar\omega)$ by the optical theorem, and the real part $f'(\hbar\omega)$ is obtained by the KK transform

$$f'(\hbar\omega)=\frac{2}{\pi}P\int_0^\infty \frac{d\omega'\,\omega' f''(\hbar\omega)}{\omega'^2-\omega^2}', \tag{6}$$

where P indicates the Cauchy principle part of the integral in the complex ω plane.

We use the sign convention found in the physics literature, in which the Thomson scattering amplitude f_0 is explicitly negative and the real part of the resonant scattering f', which is π out of phase with f_0, is a positive cusp. Consistent with the sign conventions used by FEFF, the poles of Δf are taken to lie in the lower half of the complex ω plane, yielding the dispersion relation of Eq. (6) and upward step for f''. The difference between the sign conventions used in crystallography and in quantum mechanics has been addressed previously in the context of comparing x-ray- and neutron-resonant-scattering amplitudes,[17] but continues to be

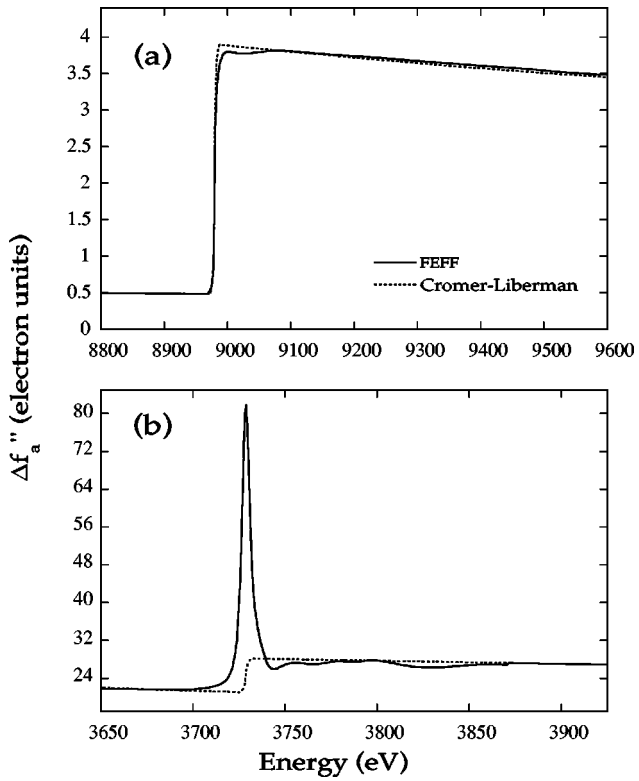

FIG. 2. Comparison between FEFF- and CL-based amplitudes $f''_a(E)$ for (a) the Cu *K*-shell resonance in Cu metal and (b) the U M_{IV} resonance in UO_2. The FEFF-based *embedded-atom* resonant scattering factors (solid lines) are generally different from the equivalent *bare-atom* functions (dashed lines) calculated by the method of Cromer and Liberman. The uranium M_{IV} resonance is an extreme example.

an issue, even in more modern calculations of the matrix elements for x-ray scattering.[18]

In principle, the dispersion relations are only valid for forward scattering. A more general expression for the optical theorem in three dimensions [19] can be written

$$\mathrm{Im}[\Delta f(\hbar\omega;\mathbf{k},\mathbf{k}')]=\frac{k}{4\pi}\int d\Omega'' f^*(\hbar\omega;\mathbf{k}'',\mathbf{k}) f(\hbar\omega;\mathbf{k}'',\mathbf{k}'), \tag{7}$$

where $|\mathbf{k}|=|\mathbf{k}'|=k$ and the integral is over all directions of the wave vector $\mathbf{k}''$. Within the dipole approximation, the angular dependence of Δf_a on $\mathbf{k}$ and $\mathbf{k}'$ vanishes [15] and the one-dimensional KK dispersion relations extend to nonforward scattering. The dipole approximation is satisfied for the resonant scattering f_c from the core electrons, which have highly localized electronic wave functions, and the off-resonance scattering, which includes a contribution from the outer shells, accounts for only a small part $\sim 10\%$ of f_a; we assume that the $\mathbf{k}$ dependence of f_{off} can be neglected. Although we neglect the complex conjugate of the leading resonant scattering term, which is required for strict analyticity, we argue that because the range of the fine structure is limited to within 1200 eV of resonance, and because nonlocal effects fall off with $1/(\omega^2-\omega_0^2)$, the difference KK is insensitive to differences between the background functions and the true analytic functions far from resonance. The $\hat{\mathbf{e}}$ and $\hat{\mathbf{e}}'$ polarization dependence of χ, introduced by the local environment of the resonant atom, is calculated explicitly in the path formalism.

The infinite range of the integral, Eq. (6), is impractical for measurement and computation. Diffraction data as a continuous function of energy are seldom collected beyond 2000 eV in a single scan, and our calculations are limited to the range over which the data are collected. FEFF does not calculate f''_c below threshold E_0, and the multiple-scattering calculation begins to diverge by about 2000 eV above E_0. Fortunately, the fine structure and other features due to solid-state effects have a limited energy range, and the atomic calculations are generally in good agreement with experimental data except in the immediate vicinity of the absorption edges. Because the difference function $\Delta f-\Delta f_a$ is nonzero over a limited energy range, the linearity of the Reimann integral allows us to write

$$f'(E)=\frac{2}{\pi}\mathrm{P}\int_0^\infty \frac{\epsilon f''(\epsilon)d\epsilon}{\epsilon^2-E^2} \tag{8a}$$

$$=\frac{2}{\pi}\mathrm{P}\int_0^\infty \frac{\epsilon\{f''_a(\epsilon)+[f''(\epsilon)-f''_a(\epsilon)]\}d\epsilon}{\epsilon^2-E^2} \tag{8b}$$

$$=f'_a(E)+\frac{2}{\pi}P\int_{\Delta E}\frac{\epsilon[f''(\epsilon)-f''_a(\epsilon)]d\epsilon}{\epsilon^2-E^2}, \tag{8c}$$

where we have changed the argument to $E=\hbar\omega$, which is more natural for synchrotron experiments. The difference KK transform (DKK) can always be exploited to reduce the infinite range of the integral KK transform when it is applied to experimental data,[20] provided Δf_a is analytic and $f''-f''_a$ vanishes outside the finite energy range ΔE. Although the atomic Δf calculated using the method of CL are not strictly analytic,[21] numerical integration in the range 5 eV to 200 keV has been used to check that the deviation from analyticity is negligible over the data range for the examples below.

In order to calculate Δf, the FEFF μ needs to agree with the background f''_a far from the absorption edge. Following standard practice in XAFS analysis, FEFF normalizes the step height in μ to unity. In addition, there may be a small linear energy dependence in the background that varies with the step size used for calculating the potentials.[22] Because of these trivial differences, we use a simple linear parametrization

$$\mu_{0,\mathrm{FEFF}}=(a_0+a_iE)\frac{f''_{c,\mathrm{CL}}}{E} \tag{9}$$

to scale the FEFF output so that it agrees with the atomic f''_c far from the edge. The atomic f''_c, which is zero below the edge, is derived from f''_a by modeling the pre-edge region f''_{off} as an Aikman polynomial [16] to subtract off the contributions from the off-resonance shells. $f''_c(E)$ and $f''_{\mathrm{FEFF}}(E)$ are then interpolated onto a uniform 1 eV grid and the numerical DKK transform of $f''_{\mathrm{FEFF}}-f''_c$ is calculated using the MacLaurin series formulation, as suggested by Ohta and Ishida.[23] The transform of the difference is then added to f'_a to obtain the FEFF-based f'. Figure 3 shows a graphical representation

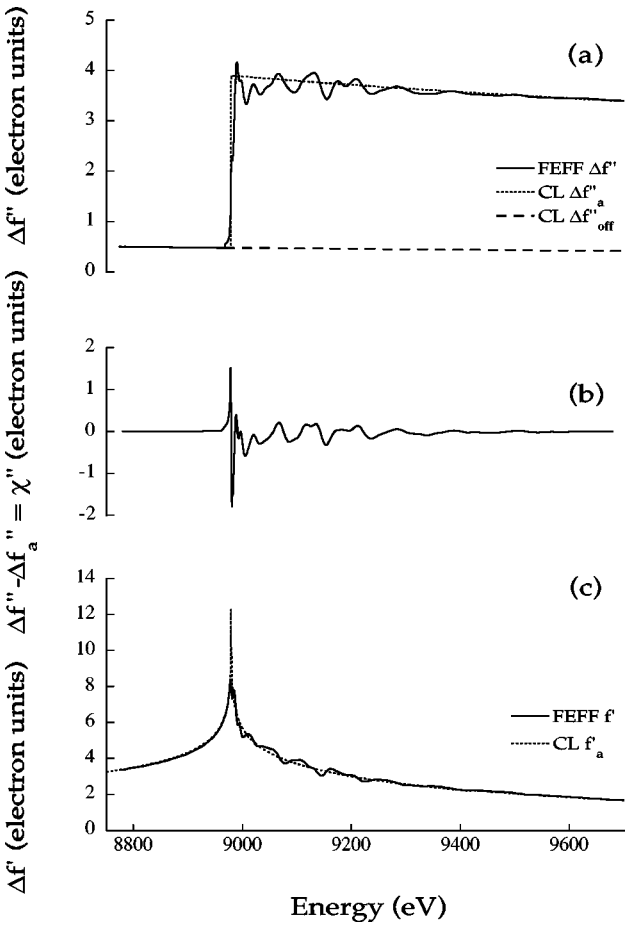

FIG. 3. The difference Kramers-Kronig transform. (a) The FEFF $\mu(E)$ is rescaled to agree with an atomic calculation of $f_c''(E)$ at high energies, then added to the contribution from the off-resonance shells $f_{\mathrm{off}}(E)$. (b) The KK transform of the difference $f''_{\mathrm{FEFF}}(E) - f_a''(E)$ is calculated using the MacLaurin series formulation (Ref. 23). (c) the transform of the difference is added to $f_a'(E)$ to obtain the FEFF-based $f'(E)$.

of the algorithm described above. Figure 3(a) shows the FEFF-based (solid line) and CL-based (dashed lines) f'', Fig. 3(b) shows the difference function $f''_{\mathrm{FEFF}} - f''_{\mathrm{CL}}$, and Fig. 3(c) shows the final FEFF-based f' (solid line) which is the sum of the CL-based f_a' (dashed line) and the DKK transform of the difference function $f''_{\mathrm{FEFF}} - f''_{\mathrm{CL}}$.

III. RESULTS

To demonstrate the accuracy of the improved theoretical amplitudes, experimentally measured Bragg peak intensities vs photon energy are compared to theoretical intensities calculated using a kinematic structure factor model with both FEFF- and CL-based Δf. In all of the theoretical calculations core-hole lifetime broadening of μ was introduced by convolution with a Lorentzian using tabulated linewidths.[24] An automated computer code, based on the DKK algorithm and using CL-based atomic calculations[25] as background functions was written for converting theoretical and experimental absorption coefficients μ into Δf, and has been made available on the internet.[26]

Experimental DAFS data from three systems are compared to kinematic structure factor calculations using CL- and FEFF-based resonant scattering amplitudes. The experiments were performed at the NSLS on beam lines X23A-2 and X22C in the vertical scattering geometry. For the theoretical calculations, we have assumed σ-σ scattering, $\hat{\mathbf{e}} = \hat{\mathbf{e}}'$, and since FEFF uses a spherical muffin-tin potential to calculate μ_0, we neglect any polarization dependence in the embedded atom Δf_a. The polarization dependence of χ for $YBa_2Cu_3O_{6.8}$ was included explicitly in the FEFF calculations.

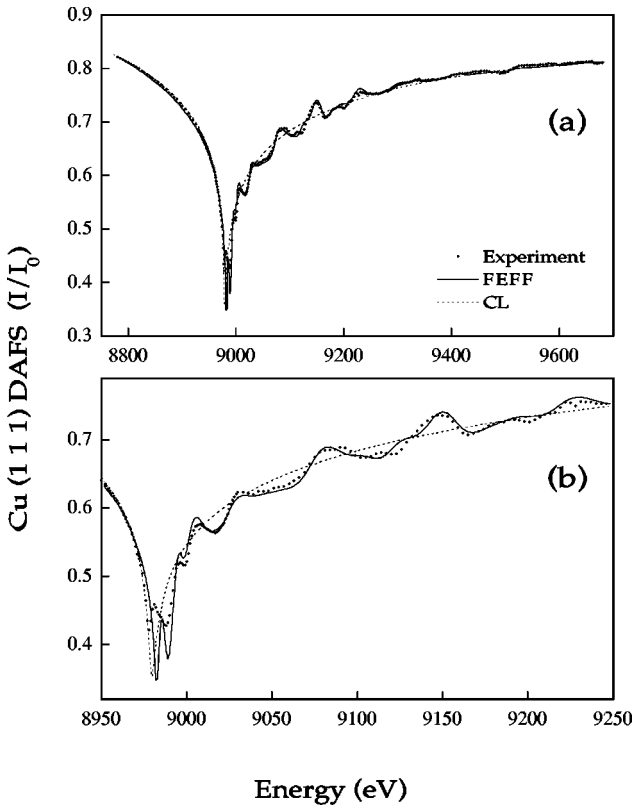

FIG. 4. Comparison between experiment (points) and theory for Cu (111) *K*-shell DAFS. Theoretical calculations for kinematic scattering with FEFF-based (solid line) and CL-based (dashed lines) Δf. The bottom figure shows an expanded view of the near-edge region.

A. Copper metal

Figure 4 shows the experimentally measured DAFS intensity for the (111) reflection of Cu metal and the theoretical intensity calculations using FEFF- and CL-based $\Delta f(E)$. The spectra were collected from a 2000-Å single-crystal film of [111] oriented fcc Cu grown by electrochemical deposition on a mica substrate.[27] The experiments were performed at NSLS beam line X23A-2 using a fixed-exit scanning monochromator[28] with Si (220) crystals. The sample was mounted in a two-circle goniometer and custom motor control software was used to track the Bragg peak θ and 2θ as the energy was scanned. The data shown in Fig. 4 are peak intensity vs angle. The full width at half maximum (FWHM) of the θ-rocking curve was 0.04°, and comparison between the ratios of peak intensity to integrated intensity at ten different energies showed less than 0.3% variation over the 1200 eV range of the scan.

The FEFF $\mu(E)$ was calculated for fcc Cu using a lattice parameter of $a=3.6148$ Å,[29] and the XAFS Debye-Waller factors were included using a correlated Debye model with $T=273$ K and $\Theta_D=315$ K.[30] All photoelectron scattering paths out to 8 Å and having 0.5% or more of the first shell scattering amplitude were included, amounting to 71 unique paths. No adjustable parameters were used in the FEFF calculation.

The FEFF-based $\Delta f(E)$ were used to calculate the theoretical intensity based on the kinematic structure factor for Cu metal according to

$$I_{\mathrm{SF}}(E,\mathbf{Q}) \propto \{[f_0(\mathbf{Q})+f'(E)]^2+[f''(E)]^2\} \times L(E,\mathbf{Q})A(E,\mathbf{Q},t), \tag{10}$$

where $\mathbf{Q}=\mathbf{k}-\mathbf{k}'$ is the wave vector transfer, $L(E,\mathbf{Q})$ is the energy-dependent Lorentz-polarization correction[31] $(E^3\sin 2\theta)^{-1}$ for σ-σ scattering at the Bragg angle 2θ, and $A(E,\mathbf{Q},t)$ is the thin-film self-absorption correction $[1-\exp\{-2\mu(E)t/\sin\theta\}]/2\mu(E)$ for a film of thickness t.[29] The theoretical intensity was scaled to the experimentally measured DAFS intensity amplitude using

$$I(E,\mathbf{Q})=a_1 I_{\mathrm{SF}}(E,\mathbf{Q})+a_2+a_3E, \tag{11}$$

where a_1 is the overall scale, and the offset a_2+a_3E allows for a small energy-dependent slope in the background. The values of a_i determined for the FEFF-based intensity were used to recalculate the intensity using CL Δf. Fig. 4(a) covers the full range of the experimental DAFS data and Fig. 4(b) shows an expanded view of the near-edge region.

The small differences between the FEFF calculation and the experimental DAFS data in Fig. 4 could be improved by varying the XAFS path parameters in a nonlinear least-squares fit; however, we have chosen to perform the calculations using only the Cu lattice parameter and Debye temperature found in the references cited above. No adjustable parameters, other than the overall scaling factors in Eq. (11), were used, in order to present a realistic result for a true *ab initio* calculation.

B. Inequivalent Cu sites in $YBa_2Cu_3O_x$

Materials with multiple inequivalent resonant sites, such as $YBa_2Cu_3O_x$, are of special interest for DAFS experiments, because the fine structure from the inequivalent sites can often be isolated crystallographically, either by finding a reflection where there is cancellation of the signal from all but one site or by making linear combinations the fine structure from several reflections. They also pose some interesting problems for MAD experiments because Δf from each site can differ dramatically, and the usual method of obtaining $\Delta f'$, by KK transform of XAFS data, can give incorrect results. Figure 5 shows the Cu *K*-shell DAFS from four of the $(00l)$ reflections of $YBa_2Cu_3O_{6.8}$, along with theoretical intensities calculated using FEFF- and CL-based Δf. The sample was a 3000 Å film of $YBa_2Cu_3O_x$ grown by pulsed laser ablation on a $10\times10\times0.5\,\mathrm{mm}^3$ MgO substrate. The *c* axis of the film was oriented normal to the surface, and the *a*-*b* plane was fully twinned. The lattice parameter $c=11.692$ Å was determined by Cu rotating anode measurements of the $(00l)$ reflections, and the oxygen depletion x

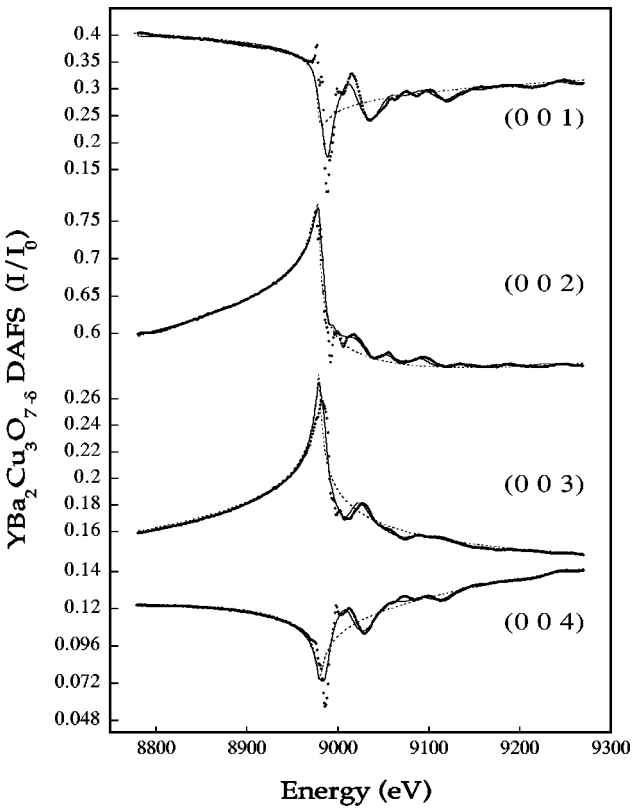

FIG. 5. $YBa_2Cu_3O_{6.8}$ *K*-shell DAFS. Comparison between experimental data (points) and theory for $(00l)$ *K*-shell DAFS from $YBa_2Cu_3O_{6.8}$. Theoretical intensities were calculated using a kinematic structure factor with FEFF-based (solid line) and CL-based (dashed line) Δf.

$=6.8$ and the in-plane lattice parameters $a=3.824$ Å and $b=3.879$ Å were estimated using the linear relationship between a, b, c, and x.[32]

The FEFF μ for the $Cu^{(1)}$ (chain) and $Cu^{(2)}$ (plane) sites were calculated separately, including the polarization dependence,[33] and the XAFS Debye-Waller factors were introduced using Einstein frequencies for the Cu-O, Cu-Ba, and Cu-Y bonds.[34,35] Since $\mathbf{Q}$ was parallel to the *c* axis, the polarization vector was confined to the twinned *a*-*b* plane for the data shown in Fig. 5. Figure 6 shows the FEFF- and CL-based f' and f'' for the two inequivalent Cu sites, as well as a sketch of the nearest-neighbor oxygen atoms. The large difference between the local environments of the two sites in the *x*-*y* plane causes a large difference in the fine structure, but no significant difference in the shape or position of the cusp and step in Δf_a, for the two sites. Because of this large difference between $\chi^{(1)}$ and $\chi^{(2)}$, reflections that would normally be forbidden for the Cu sublattice can still have a significant signal from the Cu atoms.

The ratio of the contributions from the two Cu sites at each reflection depends on the indices (hkl). Neglecting the crystallographic Debye-Waller factors, Δf for the $(00l)$ reflections may be written

$$\Delta f_l=\frac{\Delta f^{(1)}+2\cos\phi_l\Delta f^{(2)}}{1+2\cos\phi_l} \simeq \Delta f_a+f_c''\frac{\chi^{(1)}+2\cos\phi_l\chi^{(2)}}{1+2\cos\phi_l}=\Delta f_a+f_c''\chi_l, \tag{12}$$

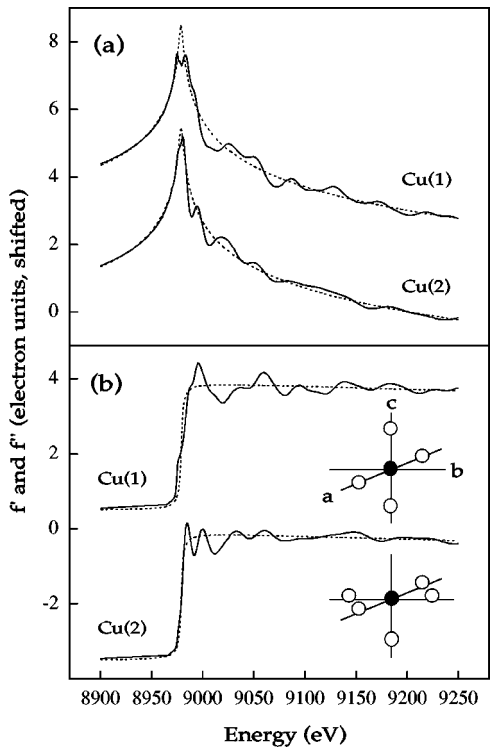

FIG. 6. Theoretical resonant scattering amplitudes (a) f' and (b) f'' for the two inequivalent Cu sites in $YBa_2Cu_3O_{6.8}$. The FEFF-based calculations (solid lines) are compared with CL-based isolated atom calculations (dashed lines). The FEFF amplitudes were calculated for vertical-plane scattering from an *a*-*b* twinned sample with the wave vector transfer parallel the *c* axis by averaging separate FEFF calculations for *a* and *b* polarization.

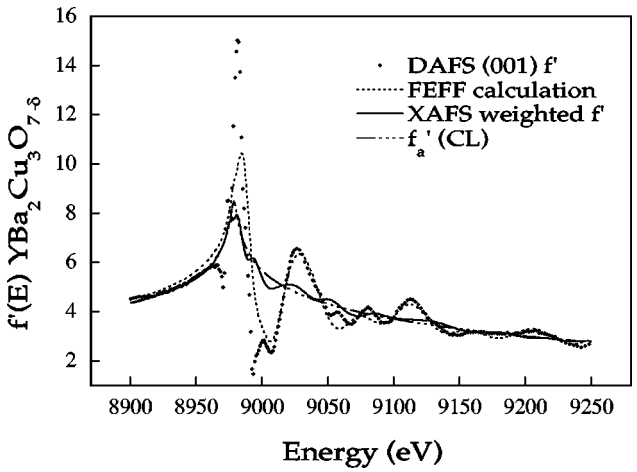

FIG. 7. Experimental DAFS-weighted f' resolved from the (001) reflection of $YBa_2Cu_3O_{6.8}$ by an iterative KK algorithm (Ref. 36) (points) compared to the crystallographically weighted FEFF calculation (dashed line), XAFS-weighted f' (solid line), and atomic f'_a (dash-dotted line). The ratio of the contributions from $Cu^{(1)}$ and $Cu^{(2)}$ is $1:1+2\cos[Qz]$ for the $(00l)$ DAFS and 1:2 for the XAFS. This illustrates the potential problem with using XAFS data to obtain near-edge resonant scattering amplitudes for multiple-site materials. The effect is strongest at forbidden or near-forbidden reflections and when the local environments of the inequivalent sites are very different.

where $\phi_l = \mathbf{Q}\cdot\mathbf{R} = 2\pi l/c$ for the $(00l)$ Bragg peaks. Equation (12) is only approximate, since any site dependence in Δf_a and f''_c has been ignored; however, this is a reasonable approximation for estimating the overall shape of $I(E,\mathbf{Q})$ since the gross features of Δf_a, i.e., the cusp depth, step height, and edge position, depend the physics of the core electron, and only weakly on the configuration of the neighbors. Changes in valence state have been observed to cause shifts in the position of the edge, sometimes quite dramatically;[3] however, the gross shape remains unchanged. We make the assumption that the DKK transform still holds in the presence of a small edge shift between the two sites, and that the difference between the shifted and unshifted $\Delta f''$ transforms correctly to the difference in $\Delta f'$, as demonstrated elsewhere.[36] At fixed $\mathbf{Q}$, all of the angular dependence in Eq. (12) is confined to the effective fine structure $\chi_l(E)$, which is the crystallographically weighted sum of $\chi(E)$ from the resonant sites.

When all of the resonant sites have the same local environment, then χ_l is the same for every Bragg reflection. This can be seen by factoring out Δf in Eq. (12) when $\Delta f^{(1)} = \Delta f^{(2)}$. The normalization of χ_l in Eq. (12) determines the relative amplitude of the fine structure with respect to the cusp depth and step height. The function Δf_l is the *effective* anomalous scattering amplitude, normalized to the single-atom response. In terms of Δf_l, the structure factor for a multiple-site material can be rewritten as

$$F = \sum_j (f_{0,j} + \Delta f_l) e^{i\mathbf{Q}\cdot\mathbf{R}_j}, \tag{13}$$

treating all of the resonant atoms as equivalent with the anomalous scattering correction Δf_l. This formalism is useful for interpreting the information content of the DAFS from materials with multiple resonant sites in the unit cell. By comparison, the normalized XAFS $\chi(E)$ is weighted according to the stoichiometry of the unit cell $\chi = \frac{1}{3}\chi^{(1)} + \frac{2}{3}\chi^{(2)}$ in this example; therefore, calculating Δf by KK transform of XAFS data can give inaccurate results.

Figure 7 shows the experimental f' for the weak (001) reflection from $YBa_2Cu_3O_{6.8}$, resolved by an iterative KK algorithm,[6,36] along with theoretical calculations of f' using the DAFS structure-factor weighting (dashed line), the XAFS 1:2 weighting (solid line), and the bare-atom CL amplitude (dot-dashed line). When the resonant atoms sit in inequivalent crystallographic sites, reflections that are normally forbidden due to destructive interference between the inequivalent sites may be allowed near resonance, as seen here. This *beating* between inequivalent resonant sites has been suggested as a possible tool for macromolecular phasing.[37,38] If the cancellation occurs within a sublattice of equivalent sites, however, this enhancement of the fine structure does not occur. In ferrite spinel (Fe_3O_4), for example, which has Fe atoms in tetrahedrally and octahedrally coordinated sites, the partial sum over the octahedral Fe sites vanishes for some reflections, independent of the sum over the tetrahedral Fe sites, and likewise for the converse. Thus, while the fine structure may be different for the two Fe sites in Fe_3O_4, it always diminishes in proportion to the gross features of Δf and therefore is not enhanced relative to Δf at weak reflections. In $YBa_2Cu_3O_{6.8}$, however, due to the low

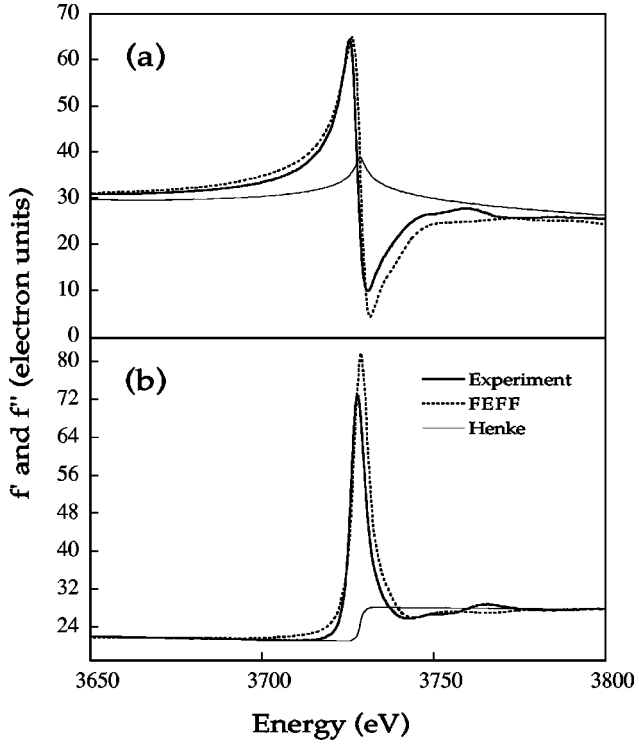

FIG. 8. Theoretical (a) $f'(E)$ and (b) $f''(E)$ for UO_2 at the U M_{IV} edge. The large white line observed in f'', which is proportional to the absorption cross section, is accompanied by a large derivativelike feature in f'. The FEFF-based resonant scattering amplitudes (solid lines) are a significant improvement over the tabulated atomic calculations (dashed lines).

symmetry of $Cu^{(1)}$, all of the reflections with weak Cu scattering give interference between the two different Cu sites.

C. Uranium oxide

X-ray resonant magnetic scattering makes use of large changes in Δf around the L and M shells of the actinides and rare-earth metals to enhance the magnetic Bragg peaks in materials with ordered moments[39–41] and to increase the surface sensitivity of magnetic scattering.[42] The white line in f'', Fig. 8(b), and the commensurate feature in f', Fig. 8(a), reflect the large number of unoccupied final states available to the outgoing photoelectron. With a white line on the order of 40 times the f'' step height, the M_{IV}-shell resonance of uranium oxide is a dramatic example of the inadequacies of atomic calculations of the anomalous scattering amplitudes.

Figure 9 shows the energy-dependent Bragg peak intensity from the (002) reflection of UO_2 around the M_{IV} absorption edge, along with FEFF- and CL-based intensity calculations. The sample was cut from a single oriented crystal to obtain a (110) surface, and the details of the surface preparation and diffraction experiment are given elsewhere.[43] The DAFS was measured as I_{peak} vs energy, and corrected for secondary extinction using the integrated θ rocking curve at several energies. The FEFF $\mu(E)$ was calculated for UO_2 using the CaF_2 structure with a lattice parameter of $a = 5.47$ Å. The XAFS Debye-Waller factors were ignored and instrument broadening was introduced by convolution with a 3 eV Lorentzian. The background functions used in the DKK

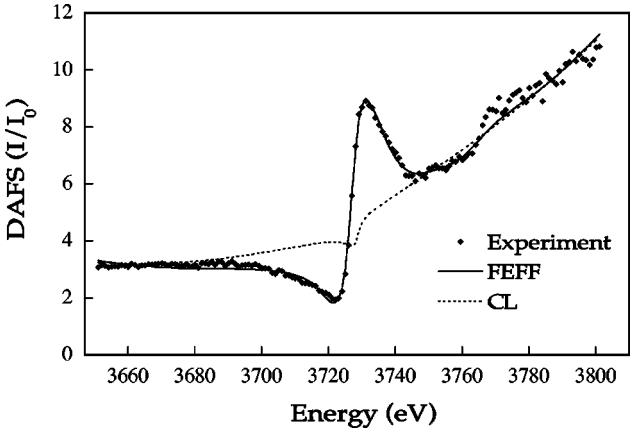

FIG. 9. Comparison between experimental data (points) and theoretical intensity calculations, using FEFF-based (solid line) and atomic (dashed line) scattering amplitudes, for UO_2 (0,0,2) DAFS at the U M_{IV} shell. The DAFS data were measured as I_{peak} vs energy, and corrected for secondary extinction using the integrated θ rocking curve at several energies.

transform were obtained by numerical integration of f_a'' from tables[44] over the tabulated range 29–30 000 eV to obtain f_a' in the vicinity of the M_{IV} edge.

It is well known that the standard tables of Δf are not useful for materials that exhibit a large white line, and, for this reason, f'' is usually determined by measuring the fluorescence XAFS spectrum and then taking the KK transform to obtain f'. When the product μt is changing by an order of magnitude, however, as in the U M_{IV} example given here, fluorescence measurements provide a poor estimate of $\mu(E)$, since the effective thickness of the sample, which, for thick samples, determines the number of absorbers, varies inversely with the cross section. This *thickness effect* is well known in XAFS and, in extreme cases, can nearly suppress the fine structure.[11] Additional x-ray-absorption data were collected on polycrystalline UO_2 around the U M_{IV} absorption edge at NSLS beam lines X24C with a fixed-exit Si (1,1,1) monochromator. Transmission, electron-yield, and fluorescence XAFS data were collected under vacuum from three polycrystalline UO_2 films of 3000 Å, 6000 Å, and 10 000 Å deposited by sputtering U metal onto a 75 μm Be substrate in an oxygen-rich reaction atmosphere. Transmission and *e*-yield data from all three films were compared to ensure the absence of self-absorption effects in the experimentally determined cross section. Transmission through a bare Be substrate was measured independently to determine the background for μ_{trans}. Figure 10 shows the U M_{IV} f'' from the 3000 Å film collected in transmission and fluorescence modes, as well as the tabulated values. The thickness effect causes a factor of 2 error in the experimental fluorescence cross section at the white line.

IV. CONCLUSION

We have demonstrated that theoretical x-ray-absorption cross sections calculated using the computer program FEFF can improve theoretical resonant x-ray-scattering amplitudes by including spectral features that are not accounted for in existing atomic codes. Although the discussion has been lim-

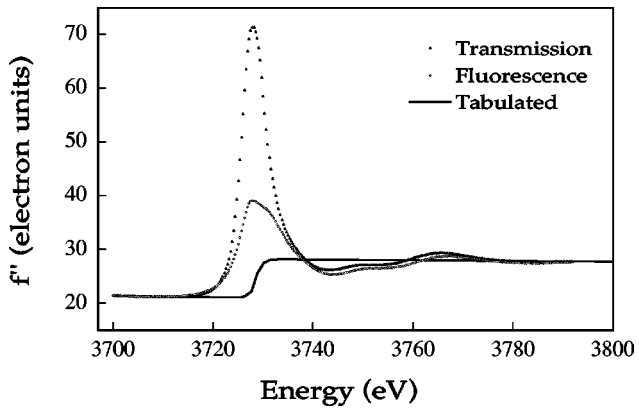

FIG. 10. Experimental f'' from XANES measurements of UO_2 at the U M_{IV} absorption edge. Comparison between XANES measurements made in electron yield (triangles) and fluorescence (circles) demonstrate how the white line is reduced by self-absorption. The bare-atom f'' convolved with a 3 eV Lorentzian (solid line) is shown for comparison.

ited to σ-σ scattering, versions of FEFF7.02 and higher have the ability to calculate the full tensor polarization dependence of the scattering $\chi(E)$ by changing the photon polarization state in the termination matrix on the final leg of each photoelectron-scattering path. As we have tried to emphasize throughout this work, the polarization dependence of Δf, which goes as $(\hat{\mathbf{e}}\cdot\hat{\mathbf{r}}_1)(\hat{\mathbf{e}}'\cdot\hat{\mathbf{r}}_N)$ in the path formalism, where $\mathbf{r}_1$ and $\mathbf{r}_N$ indicate the first and final legs of the path, is different from the polarization dependence of the Thomson scattering amplitude, which goes as $\hat{\mathbf{e}}\cdot\hat{\mathbf{e}}'$, and from the polarization dependence of the XAFS, which goes as $(\hat{\mathbf{e}}\cdot\hat{\mathbf{r}}_1)(\hat{\mathbf{e}}\cdot\hat{\mathbf{r}}_N)$. This suggests that it may be possible to observe small changes in the relative intensities of the Bragg peaks that are not in agreement with structure factor calculations, but that can be interpreted in terms of the XAFS path formalism, by collecting resonant scattering spectra at out-of-plane reflections from materials where local environment of the resonant atoms has low symmetry. We are not aware of any work on this specific topic; however, the tensor polarization dependence of Δf from materials which exhibit quadrupole scattering has been found experimentally to be small.[20,45,10]

A larger effect, and one that we believe warrants consideration for resonant scattering experiments from all materials with multiple inequivalent sites, is the possibility of strong enhancement of the fine structure at reflections that are forbidden, or nearly forbidden, due to cancellation between inequivalent resonant sites. The effect occurs when cancellation in the structure factor requires mixing amplitudes from inequivalent sites with very different local environments, as illustrated by the example given in Fig. 7 for the weak (001) reflection from $YBa_2Cu_3O_{6.8}$.

As a final note, we would like to point out that in order to calculate the x-ray-absorption cross sections, FEFF uses a sophisticated and fast atomic potential algorithm to calculate the electron density around the embedded central atom. With the standard approximation of spherical symmetry, this electron density can be used to calculate the Thomson scattering $f_0(\mathbf{Q})$ by direct Fourier transform. Using the overlapped atomic calculations of of FEFF7, $f_0(\mathbf{Q})$ has been reproduced[46] to within $\sim$2% of values given in standard tables.[47] Work is now being done to make the atomic potentials of FEFF consistent with the photoelectron scattering potentials,[48] which should give better calculations of $f_0(\mathbf{Q})$ for atoms embedded in real solids.

ACKNOWLEDGMENTS

The authors would like to acknowledge H. Stragier, C. C. Bitz, and J. C. Woicik for their participation in the Cu and $YBa_2Cu_3O_{6.8}$ DAFS experiments; J. C. Woicik for his assistance with the UO_2 XAFS measurements at NSLS X24 A; and D. Yee and M. Toney for providing the Cu crystal. This work was partially supported by the Office of Naval Research. The experiments were carried out at the National Synchrotron Light Source, Brookhaven National Laboratory, which is supported by the U.S. Department of Energy, Division of Materials Sciences and Division of Chemical Sciences.

APPENDIX: DERIVATION OF THE DAFS FINE-STRUCTURE COEFFICIENT

The absorption cross section of Eq. (2) is typically calculated using a Green's function formalism, which has a physical interpretation as a sum over photoelectron-scattering paths. Since the final states ψ_f in Eq. (2) are identical to the intermediate states ψ_n in Eq. (1), the same formalism and interpretation also apply to the resonant scattering amplitude. Replacing the sum over intermediate states by the one-particle retarded Green's function

$$G^+(\mathbf{r},\mathbf{r}')=\sum_n \frac{|\psi_n\rangle\langle\psi_n|}{E-E_n+i\eta}, \tag{A1}$$

where of all the dissipative terms, including the core-hole lifetime $\frac{1}{2}\Gamma_n$ and the lossy part of the potential, are lumped together in a net η, Eq. (1) becomes

$$\Delta f(E)=-\left(\frac{e}{mc}\right)^2\langle\psi_i|\hat{\mathbf{e}}'^*\cdot\mathbf{r}'\,G^+(\mathbf{r},\mathbf{r}')\hat{\mathbf{e}}\cdot\mathbf{r}|\psi_i\rangle, \tag{A2}$$

which, except for the polarization dependence noted above, is closely related to the expression for the x-ray-absorption coefficient:

$$\mu(E)=-\frac{4\pi\hbar\alpha}{\omega m^2}\mathrm{Im}[\langle\psi_i|\hat{\mathbf{e}}^*\cdot\mathbf{r}'\,G^+(\mathbf{r},\mathbf{r}')\hat{\mathbf{e}}\cdot\mathbf{r}|\psi_i\rangle]. \tag{A3}$$

The sum is taken over empty final states, so that $G^+(\mathbf{r},\mathbf{r}')$ implicitly includes the Fermi-Dirac function $\Theta(E_f-E)$. Separating $G^+(\mathbf{r},\mathbf{r}')$ into central embedded-atom $G_c^+(\mathbf{r},\mathbf{r}')$ and photoelectron scattering $G_{sc}^+(\mathbf{r},\mathbf{r}')$ terms and expanding over angular momentum states L of the outgoing photoelectron, the central-atom contribution can be written

$$G_c^+(\mathbf{r},\mathbf{r}')=\sum_L R_L(\mathbf{r}_<)R_L^+(\mathbf{r}_>) \tag{A4}$$

as in the multiple-scattering (MS) theory of XAFS.[49] R_L is a solution to the radial Shrödinger equation,[50] $\mathbf{r}_>$ and $\mathbf{r}_<$ refer to the greater and lesser of $\mathbf{r}$ and $\mathbf{r}'$, respectively, and $R_L(\mathbf{r})=R_L(\mathbf{r})Y_L(\hat{\mathbf{r}})$. The remaining photoelectron scattering terms can be written

$$G^+_{sc}(\mathbf{r},\mathbf{r}')=\sum_{L,L'} R_L(\mathbf{r})R_{L'}(\mathbf{r}')G^+_{L,L'}(\mathbf{r},\mathbf{r}'). \qquad \text{(A5)}$$

Note that since $\mathrm{Im}[R^+_L(\mathbf{r}_>)]=R_L(\mathbf{r}_<)$, both the central-atom and the scattering contributions to $\mathrm{Im}[G^+(\mathbf{r},\mathbf{r}')]$ have the same dependence of the radial wave functions, i.e., $\mathrm{Im}[G^+_c(\mathbf{r},\mathbf{r}')]=\Sigma_L R_L(\mathbf{r})R_L(\mathbf{r}')$ and $\mathrm{Im}[G^+_{sc}(\mathbf{r},\mathbf{r}')]=\Sigma_{L,L'}R_L(\mathbf{r})R_{L'}(\mathbf{r}')\mathrm{Im}[G^+_{L,L'}(\mathbf{r},\mathbf{r}')]$.

Equation (A3) can then be used to write the total absorption coefficient as $\mu_{\mathrm{tot}}=\mu_{\mathrm{off}}+\mu_0(1+\chi'')$, where $\chi''=\mathrm{Im}[G^+_{L,L'}(\mathbf{r},\mathbf{r}')]$ is the fine-structure term due to photoelectron scattering from near-neighbor atoms, μ_0 is the embedded-atom absorption coefficient due to the resonance derived from $\mathrm{Im}[G^+_c(\mathbf{r},\mathbf{r}')]$, and μ_{off} is the smooth absorption coefficient from the excitation of lower-energy levels. Since f'' and μ are related by the optical theorem at $\mathbf{k}=\mathbf{k}'$, it follows that $f''=f''_{\mathrm{off}}+f''_c(1+\chi'')$ where $f''_c\propto\mu_0$ and $f''_{\mathrm{off}}\propto\mu_{\mathrm{off}}$. In contrast, $f'=f'_{\mathrm{off}}+f'_c+f''_c\chi'$, where $\chi'=\mathrm{Re}[G^+_{L,L'}(\mathbf{r},\mathbf{r}')]$ and f'_{off} is the real part of the anomalous scattering from resonances of other core levels. The prefactor to χ' follows directly from both the real and imaginary parts of $G^+_{sc}(\mathbf{r},\mathbf{r}')$ above depending on $R_L(\mathbf{r})R_{L'}(\mathbf{r}')$, which is proportional to $-\mathrm{Im}[G^+_c(\mathbf{r},\mathbf{r}')]$.

*Electronic address: jox@pnc.aps.anl.gov
†Current address: CARS, University of Chicago, Chicago, Illinois 60637.

[1] See, for example, articles contained in *Resonant Anomalous X-Ray Scattering: Theory and Applications*, edited by G. Materlik, C. J. Sparks, and K. Fischer (North-Holland, Amsterdam, 1994).
[2] J. Karle, Int. J. Quantum Chem. **7**, 357 (1980).
[3] W. A. Hendrickson, Science **254**, 51 (1991).
[4] H. Stragier, J. O. Cross, J. J. Rehr, L. B. Sorensen, and J. C. Woicik, Phys. Rev. Lett. **69**, 3064 (1992).
[5] L. B. Sorensen *et al.*, in *Resonant Anomalous X-Ray Scattering: Theory and Applications*, edited by G. Materlik, C. J. Sparks, and K. Fischer (North-Holland, Amsterdam, 1994), pp. 389–420. See Ref. 1.
[6] I. J. Pickering, M. Sansone, J. Marsch, and G. N. George, J. Am. Chem. Soc. **115**, 6302 (1993).
[7] L. G. Parratt and C. F. Hempstead, Phys. Rev. **94**, 1593 (1954).
[8] D. T. Cromer and D. Liberman, J. Chem. Phys. **53**, 1891 (1970).
[9] J. Bohr, D. Gibbs, and K. Huang, Phys. Rev. B **42**, 4322 (1990).
[10] D. H. Templeton and L. K. Templeton, Phys. Rev. B **49**, 14 850 (1994).
[11] E. A. Stern and S. M. Heald, in *Handbook of Synchrotron Radiation*, edited by E. E. Koch (North-Holland, New York, 1983).
[12] *X-ray Absorption: Principles, Applications, Techniques of EXAFS, SEXAFS, and XANES*, Vol. 92 of *Chemical Analysis*, edited by D. C. Koningsberger and R. Prins (Wiley, New York, 1988).
[13] J. J. Rehr, J. M. de Leon, S. I. Zabinsky, and R. C. Albers, J. Am. Chem. Soc. **113**, 5136 (1991).
[14] S. I. Zabinsky *et al.*, Phys. Rev. B **52**, 2995 (1995).
[15] J. J. Sakurai, *Advanced Quantum Mechanics* (Addison-Wesley, Menlo Park, CA, 1997).
[16] S. Sasaki, KEK Report No. **88-14**, 1989 (unpublished).
[17] S. Ramaseshan, T.G. Ramesh, and G. S. Ranganath, in *Anomalous Scattering*, edited by S. Ramaseshan and S.C. Abrahams (Munksgaard, Copenhagen, 1975), pp. 139–161.
[18] R. H. Pratt, Lynn Kissel, and P. M. Bergstrom, Jr., in *Resonant Anomalous X-Ray Scattering: Theory and Applications*, edited by G. Materlik, C. J. Sparks, and K. Fischer (Elsevier Science, New York, 1994), pp. 9–33.
[19] M. Goldberger and K. M. Watson, *Collision Theory* (Wiley, New York, 1964).
[20] L. K. Templeton and D. H. Templeton, J. Appl. Crystallogr. **21**, 558 (1988).
[21] L. Kissel *et al.*, Acta Crystallogr., Sect. A: Found. Crystallogr. **51**, 271 (1995).
[22] The integral step size for calculating the phases in FEFF can be changed using the RGRID card. A smaller value will give better results, but also makes the calculation slower.
[23] K. Ohta and H. Ishida, Appl. Spectrosc. **42**, 952 (1988).
[24] O. Keski-Rahkonen and M. O. Krause, At. Data Nucl. Data Tables **14**, 140 (1974).
[25] S. Brennan and P. L. Cowan, Rev. Sci. Instrum. **63**, 850 (1992).
[26] http://cars1.uchicago.edu:80/newville/dafs/diffkk, download site for the FORTRAN source code for DIFFKK, to convert FEFF absorption cross sections μ into resonant scattering amplitudes Δf.
[27] M. F. Toney *et al.*, Phys. Rev. Lett. **75**, 4472 (1993).
[28] J. A. Golovchenko, R. A. Levesque, and P. L. Cowan, Rev. Sci. Instrum. **52**, 509 (1981).
[29] B. D. Cullity, *Elements of X-Ray Diffraction* (Addison-Wesley, Menlo Park, CA, 1978).
[30] N. W. Ashcroft and N. D. Mermin, *Solid State Physics* (Holt, Rinehart and Winston, New York, 1976).
[31] R. W. James, *The Optical Principles of the Diffraction of X-rays* (Ox Bow Press, Woodbridge, CT, 1962).
[32] J. D. Jorgensen *et al.*, Phys. Rev. B **41**, 1863 (1990).
[33] The FEFF polarization card was used with the arguments ELLIPTICITY 1 0 0 1 and POLARIZATION 1 1 0, to simulate the average of *a* and *b* polarization from the twinned crystal.
[34] C. Y. Yang *et al.*, Phys. Rev. B **38**, 6568 (1988).
[35] D. Haskel (private communication).
[36] J. O. Cross, Ph.D. thesis, University of Washington, 1996.
[37] D. H. Templeton and L. K. Templeton, Acta Crystallogr., Sect. A: Found. Crystallogr. **47**, 414 (1991).
[38] C. E. Bouldin, L. B. Sorensen, H. J. Stragier, and B. D. Ravel (unpublished).
[39] D. Gibbs, J. Less-Common Met. **148**, 109 (1989).
[40] W. G. Stirling and G. H. Lander, J. Appl. Phys. **73**, 6877 (1993).
[41] C. Detlefs *et al.*, Phys. Rev. B **55**, R680 (1997).
[42] G. M. Watson *et al.*, Phys. Rev. Lett. **77**, 751 (1996).
[43] G. M. Watson *et al.*, Phys. Rev. B **53**, 686 (1996).
[44] B. L. Henke, E. M. Gullikson, and J. C. Davis, At. Data Nucl. Data Tables **54**, 181 (1993); tabulated data are available on-line at http://xray.uu.se/hypertext/ptable.html.
[45] D. H. Templeton and L. K. Templeton, Acta Crystallogr., Sect. A:

Found. Crystallogr. **48**, 746 (1992).
[46] M. Newville *et al.* (unpublished).
[47] D. Rez, P. Rez, and I. Grant, Acta Crystallogr., Sect. A: Found. Crystallogr. **50**, 481 (1994).
[48] A. L. Ankudinov (private communication).
[49] J. Rehr, R. Albers, and S. Zabinsky, Phys. Rev. Lett. **69**, 3397 (1992).
[50] K. Göttfried, *Quantum Mechanics* (Benjamin, New York, 1966).